J Fail. Anal. and Preven. (2023) 23:497–510
https://doi.org/10.1007/s11668-022-01575-7

TECHNICAL ARTICLE—PEER-REVIEWED

Rupture Life and Failure Mechanism of Grade 91 Steel Under the Influence of Notch Constraint

Imam Ul Ferdous · N. A. Alang · J. Alias · A. H. Ahmad · Suraya Mohd Nadzir

Submitted: 9 September 2022 / in revised form: 7 December 2022 / Accepted: 9 December 2022 / Published online: 23 December 2022

Abstract Coal-fired power plants must operate at higher temperatures and pressures to achieve maximum efficiency. During operation, components are exposed to the creep environment, which can lead to catastrophic plant failure. In this study, an initiative was taken to evaluate the creep behavior and failure mechanism of Grade 91 steel by conducting creep tests at 873 K and different stress levels. Two types of specimens (smooth and notched) were used to study the effects of uniaxial and multiaxial stress states on creep strength. Notched specimens with different acuities (2.28 and 4.56) were employed. The creep curve of both specimens showed all three stages known as primary, secondary, and tertiary. The secondary stage seems to be dominant in all three. The analysis of the creep life under the influence of net stress showed that the notched specimen had a longer creep life than the smooth specimen at the same stress level, indicating a "notch strengthening" effect. The effects of the representative stress were also evaluated, revealing that the von-Mises stress controls the rupture life. A comparative analysis of multiaxial ductility is made with various void-growth models. The Rice and Tracey model closely matches the experimental data at lower triaxiality, but the Cocks and Ashby and Splinder model overestimates the ductility. The fractography examination of the notched specimen revealed that, in comparison to the area at the root, the area towards the middle of the notch exhibits shallow dimples, indicating less plasticity. Meanwhile, the ruptured surface of smooth specimens shows that ductile dimples predominate.

Keywords Creep damage · Grade 91 steel · Notch constraint · Notch acuity · Rupture life

This article is an invited paper selected from presentations at the 6th Symposium on Damage Mechanism in Materials and Structures (SDMMS 2022), held August 16–17, 2022 in Kuantan, Malaysia. The manuscript has been expanded from the original presentation. The special issue was organized by Nasrul Azuan Alang, Norhaida Ab Razak, and Aizat Alias, Universiti Malaysia Pahang.

I. U. Ferdous · N. A. Alang (✉)
Structural Performance and Materials Engineering (SUPREME) Focus Group, Faculty of Mechanical and Automotive Engineering Technology, Universiti Malaysia Pahang, Pekan, Pahang, Malaysia
e-mail: azuan@ump.edu.my

J. Alias · A. H. Ahmad
Department of Mechanical Engineering, College of Engineering, Universiti Malaysia Pahang, Gambang, Kuantan, Pahang, Malaysia

S. Mohd Nadzir
TNB Research Sdn Bhd, No. 1, Lorong Air Itam, Kawasan Institut Penyelidikan, Kajang, Selangor, Malaysia

Introduction

In the field of power generation, one of the main objectives is to achieve maximum efficiency, which largely depends on the operating conditions of the plant. The goal in developing alloys for use at high temperatures is to withstand the operating conditions for the duration of the service life. In addition, optimal maintenance costs can be achieved by using low-cost materials for manufacturing equipment and components. Due to improved mechanical properties and reasonable price, martensitic heat-resistant steels with high Cr content have gradually replaced austenitic stainless steels as a core element for ultra-supercritical (USC) power plants [1]. Grade 91 steel is a potential candidate to meet the underlying requirements

among the available high Cr steels. Since it has improved creep resistance over low-alloy steels such as 2.25Cr-1Mo steel and better thermo-physical properties, Grade 91 steel is now widely used in pressure vessels and piping systems in the petrochemical industry and fossil fuel power plants with steam temperatures up to 873 K [2]. Compared to austenitic steels such as 300 series stainless steel, Grade 91 Steel has relatively low thermal expansion and higher thermal conductivity [3].

With long-term use, creep rupture occurs at the microstructural level under the influence of the creep environment, resulting in cracks and a loss of load-bearing capacity. The creep test contributes to understanding creep behavior and is also essential for deriving the constitutive creep model, which is the prerequisite for predictive modeling. However, determining the exact creep mechanism at rupture is difficult because it is temperature and stress level dependent. In recent years, numerous uniaxial creep tests have been carried out on Grade 91 steel at different stress levels. Due to various factors, such as changes in geometry, inhomogeneous microstructure (e.g., welds), or types of loading during operation, multiaxial stresses are generated in components. Although creep data obtained under uniaxial loading is often used in the design process, it is better to understand creep behavior under multiaxial loading. Multiaxial stresses are usually induced in power plant components at the stress-concentrated location, which diverges the creep deformation [4].

The creep and rupture behavior of materials under multiaxial conditions can be studied with notched specimens [5]. The material's degree of constraint is determined by the type of notch used, the notch root profile, and the material's creep ductility [6]. U-type and V-type notches can be used to explore the influence of constraint on creep deformation and rupture. The U-type notches are preferred over the V-type notches because the U-notches cause creep damage across a larger area, making the investigation easier [6]. Depending on the multiaxial condition of stress across the notch throat plane and the ductility of the material, notch strengthening or notch weakening may occur [7]. Due to the rapid stress redistribution in the notch plane, notches are predicted to strengthen the structure under creep conditions [8]. The strengthening effect is often observed in relatively ductile materials. Nevertheless, notch weakening is likely to occur in cases where axial stress redistributes slowly over time due to the presence of the notch. Creep voids will form near the notch root because of the stress concentration. Brittle materials tend to have this tendency [9]. However, the assessment of notch strengthening or notch weakening behavior is critical in the design and manufacture of parts, and it must be confirmed that the selected material has a notch strengthening effect in service. For this reason, many studies still need to be done to find out how notches affect creep damage and the rupture of materials.

Changes in the creep mechanism under the influence of multiaxial stresses must be considered when assessing the damage. Goyal et al. [10] studied the creep and rupture behavior of notched and smooth 9Cr–1Mo steel specimens. Their studies showed that the creep strength of steel improves with increasing degrees of notch constraint and that the creep ductility of steel decreases under conditions of decreasing notch constraint. In another study [11], the degree of notch constraint was found to strongly influence the propagation of creep damage.

Conducting the creep test under the same conditions to which the component is subjected in service would be costly, time-consuming, and inefficient. Therefore, creep tests in the laboratory are usually carried out at higher stresses to shorten the test duration, and the data obtained are used to predict long-term creep behavior [12]. At higher stress levels, dislocation or power-law creep dominates, while at lower stress levels, diffusion creep takes control, affecting the slope of the stress versus time curve. Analysis of failure strain with respect to creep ductility and reduction of area can contribute to a better understanding of creep behavior and the influence of the notch on creep rupture life. At high stresses, dislocation predominated over creep, resulting in transgranular fractures with significant plastic deformation and ductile dimples [13]. Intergranular fracture with a low degree of deformation occurs at low stress or over a substantially more extended period of time when diffusional creep occurs [14].

Due to the complex stress distribution caused by the notch, the representative stress can be used instead of the net section stress to better express the creep behavior. Hayhurst [15] showed how the multiaxial stress is affected by von-Mises, the maximum principal stress (MPS), hydrostatic stresses, or a combination of the three and offered a parameter to control the bias mechanism. The von-Mises stress is assumed to govern the rupture life at higher stresses, while the MPS governs damage propagation at lower stresses. Chang et al. [16] conducted an experiment on P92 steel regarding representative stresses and found that the concept was suitable for estimating creep life under a multiaxial stress condition.

Various models of void growth, such as Rice and Tracey [17], Cocks and Ashby [18], and Spindler [19], can be used to establish a relationship between multiaxial stress and creep ductility. They showed that the ratio of multiaxial ductility to uniaxial ductility is a function of the ratio of hydrostatic to equivalent stress, known as the triaxiality factor. According to these models, there is an inverse relationship between creep ductility and triaxiality, suggesting that as stress increases, ductility also decreases.

In this work, an attempt was made to characterize the creep behavior and failure mechanism of Grade 91 steel at 873 K. The effect of notch constraint on creep strength was quantified by performing a series of creep tests on the notched specimens with different acuities. Fractographic analysis of the crept sample was performed to investigate the possible damage mechanism. The author believes that the data collected in this study will help to determine the material parameters that are prerequisites for the formulation of a constitutive model to predict creep damage as well as to better understand the creep damage mechanism under multiaxial stress state condition.

Material and Method

Chemical Composition

The chemical composition of Grade 91 steel was determined by Optical Emission Spectroscopy (Foundry Master Oxford Instruments) on a cylindrical, grinded, and polished 20 mm sample taken from the as-received pipe block. The reading was performed at five different points, and the average values were calculated. Table 1 tabulates the chemical composition of the material.

Microstructure

A sample with a diameter of 10 mm and a height of 10 mm was cut from Grade 91 pipe in the as-received condition. The sample was hot mounted and prepared for further microscopic examination. A thermosetting plastic material (Bakelite) was used to embed the sample. The mounted specimen was ground with sandpaper of different grits (#320, #400, #600, #800, #1200), from coarser to finer. After getting uniform grinding in one direction, the specimen was rotated 90° and moved to the next grit of sandpaper. This procedure was repeated for finer sandpapers. The specimen was first polished with a 1 µm diamond extender and DIALUBE lapping lubricant and then polished with 0.05 µm NANOPOLISH alumina and water to bring it to a mirror finish. After polishing, the polished specimen was first cleaned from grease, oil, and the polishing compound's residue, then etched with Vilella's reagent (etchant) and allowed to stand for 10–15 s before being cleaned under tap water. Drying of the specimen was done using an air gun. After etching, the specimen was observed under an optical microscope, and scanning electron microscopy (SEM), and the microstructure that appeared was captured. Microscopic examination reveals a martensitic lath structure, precipitates, and prior austenite grain boundary (PAGB) (see Fig. 1).

Table 1 Chemical Composition of Grade 91 steel

C	Si	Mn	P	S	Cr
0.108	0.410	0.380	0.003	0.005	8.790
Mo	V	Nb	N	Ni	Al
0.994	0.226	0.040	0.045	0.100	0.005

Specimen Geometry

All creep specimens were extracted in the longitudinal direction from the commercial as-received Grade 91 pipe, as shown in Fig. 2, and the geometry and the dimensions of the test specimens are presented in Fig. 3. The smooth and notched specimens have a similar total length of 92 mm, and a gauge length of 36 mm. Two different notch radii were considered in this study. The medium-notched specimen had a radius of 1.25 mm, and the blunt-notched specimen had a radius of 2.5 mm, giving the acuity ratio (the ratio between notch throat diameter and notch radius) of 2.28 and 4.56, respectively.

Creep Rupture Test

The creep test was performed according to the test procedures ASTM E139 [20] and ASTM E292 [21] for smooth and notched specimens, respectively. A dead load creep testing machine with a lever load ratio of 1:50, equipped with a cylindrical furnace to provide a controlled high-temperature environment, was used to perform the tests. The specimen was held in the furnace using the threaded specimen holder, and three K-type thermocouples were placed at different locations (top, middle, and bottom) to measure the temperature. Two gripping mechanisms were attached to the specimen and extended to the linear variable differential transformer (LVDT), as shown in Fig. 4b. All specimens were tested at 873 K, and the temperature was carefully monitored to ensure that they were within ± 2 °C throughout the test. The axial elongation of the material was measured using a pre-calibrated linear variable differential transformer (LVDT) attached with a clamp. Once all three thermocouples had reached the target temperature, a predefined load was applied. For notched specimens, the stress field, mainly in the notched region, varies with time (a process known as "stress redistribution"). Therefore, the net cross-sectional stress, defined as the average of the longitudinal stress over the entire notch neck diameter, is used to indicate the applied stress. Note that during the primary stage of deformation, creep displacement data were recorded every 2 min, and during the secondary stage, every 10 min. Figure 4 and Table 2 show

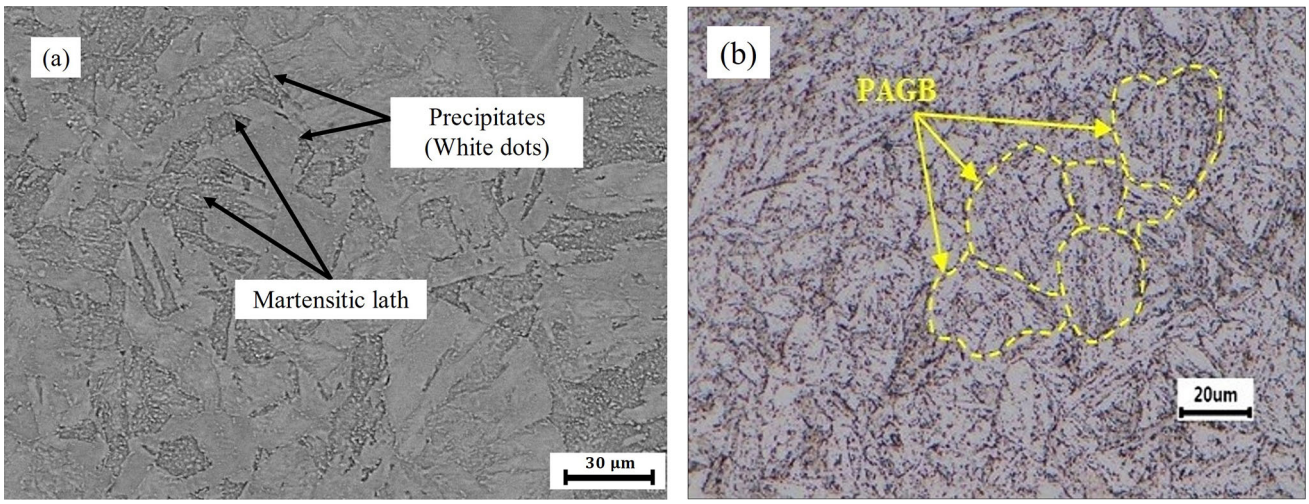

Fig. 1 (**a**) SEM micrograph of as-received Grade 91 steel, (**b**) optical micrograph of as-received Grade 91 steel

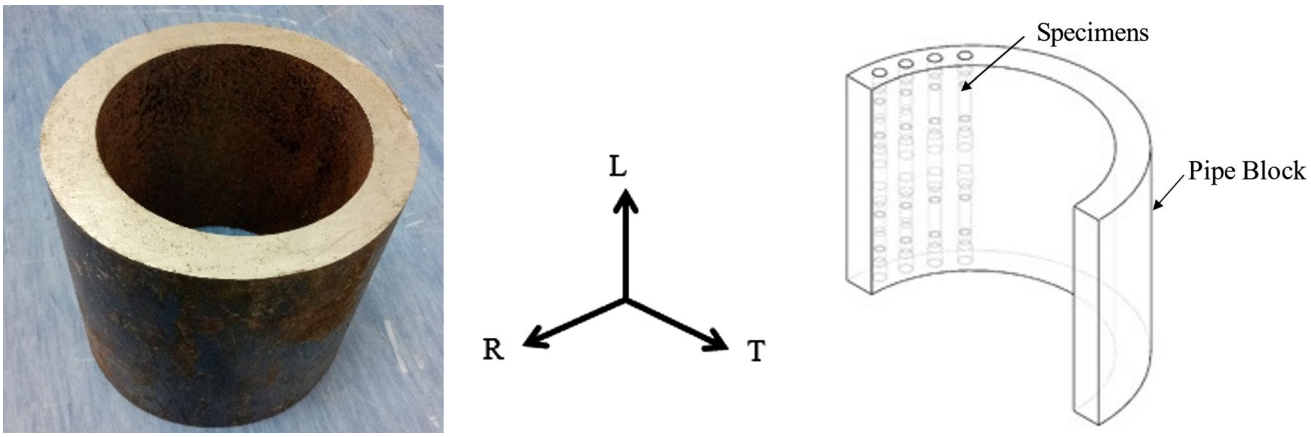

Fig. 2 (**a**) As-received commercial Grade 91 Steel pipe, (**b**) schematic diagram of the extracted specimen

the available creep testing machine at Universiti Malaysia Pahang and the test matrix for the creep test, respectively.

The LDVT collected raw data in the form of axial displacement during the test. The total change in axial length and cross-sectional area of the crept specimen was determined using a profile projector machine (10X magnification), as shown in Fig. 5a. Since the cross-sectional area is not uniform within the notched bar's gauge length, the specimen's ductility is also calculated based on the reduction of area (ROA). The schematic of the crept specimen and the dimensions used to calculate ductility and reduction of area (ROA) are shown in Fig. 6.

Ductility

To determine the ductility in terms of failure strain, the total axial displacement at rupture ($l_1 + l_2$) was measured using the profile projector. Then, using Eq. 1, the ductility was calculated.

$$\text{Ductility } (\%) = \frac{\Delta l}{l_0} \times 100 \qquad \text{(Eq 1)}$$

Here, Total length = $l_1 + l_2$, Gauge length = l_0, Axial deformation (Δl) = total length – gauge length.

Reduction of Area

Another form of failure strain, reduction of area (ROA), was determined using Eq. 2. The cross-sectional area at the rupture point was determined, and the ROA of the crept specimens was evaluated.

$$\text{Reduction of area (ROA)}\ \% = \frac{A_0 - A_f}{A_0} \times 100 \qquad \text{(Eq 2)}$$

Here, Diameter of the first crept sample at the fracture point = d_1

Diameter of the second crept sample at the fracture point = d_2

Average diameter, $d = \frac{d_1 + d_2}{2}$

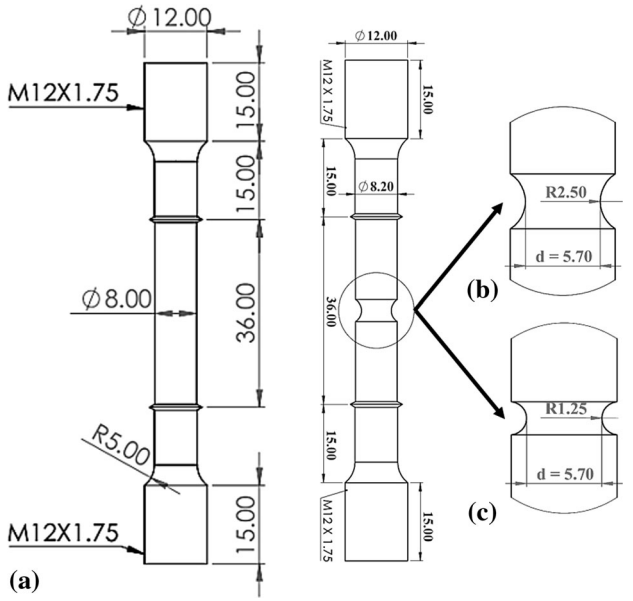

Fig. 3 Dimensions of the test specimen for (**a**) smooth, (**b**) blunt-notched, and (**c**) medium-notched

Table 2 Test matrix for creep-rupture testing

Specimen type	Temperature, T (K)	Notch radius, r (mm)	Acuity ratio (d/r)	Net stress, σ (MPa)
Smooth specimen	873	N/A	N/A	160
				170
				180
				190
Medium notched specimen		1.25	4.56	210
				220
				230
				240
Blunt notched specimen		2.50	2.28	210
				220
				230
				240

d is the ligament diameter at the notch area

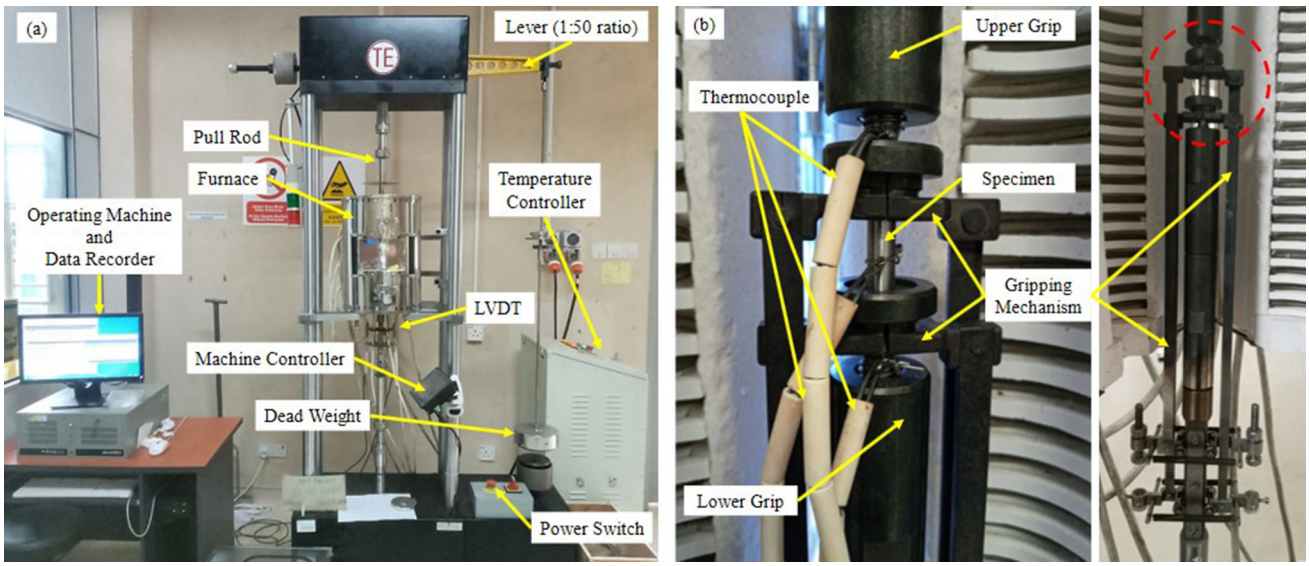

Fig. 4 (**a**) Available creep testing machine, (**b**) details of the experimental setup

Initial cross-sectional area = A_0, Final cross-sectional area, $A_f = \frac{\pi d^2}{4}$

Instead of the elongation approach, ROA allows more realistic evaluations of creep ductility because ROA measurements are made at the local fracture location. In contrast, the evaluation of ductility based on axial displacement gives the average result along the gauge length. Moreover, the axial displacement of the notched bar is non-uniform, which leads to inaccuracies in the calculation of ductility (by axial displacement).

Results and Discussion

Creep Curve

Figure 7 shows the creep strain versus time for smooth specimens subjected to stresses between 160 and 190 MPa. All specimens exhibit three stages of deformation: primary, secondary, and tertiary. In the primary stage, the material deforms at a higher strain rate at the applied load and then the strain rate slowly decreases. The material deforms at approximately 0.025–0.05 mm/mm before entering the

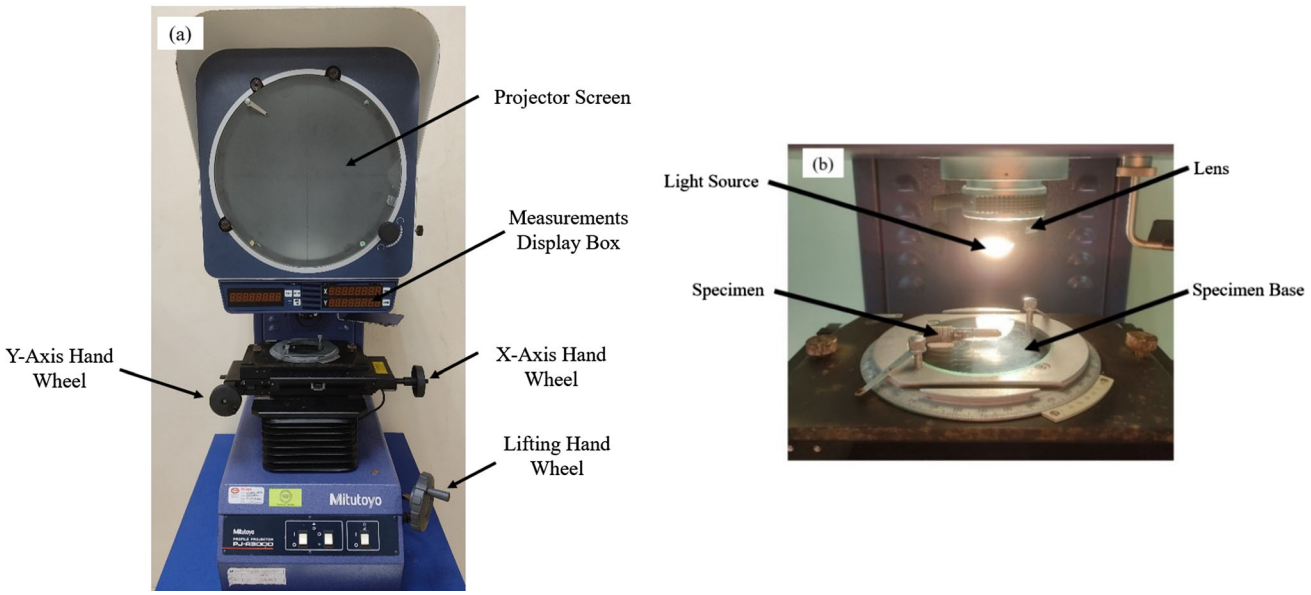

Fig. 5 (**a**) Profile projector machine, (**b**) specimen during the measurement

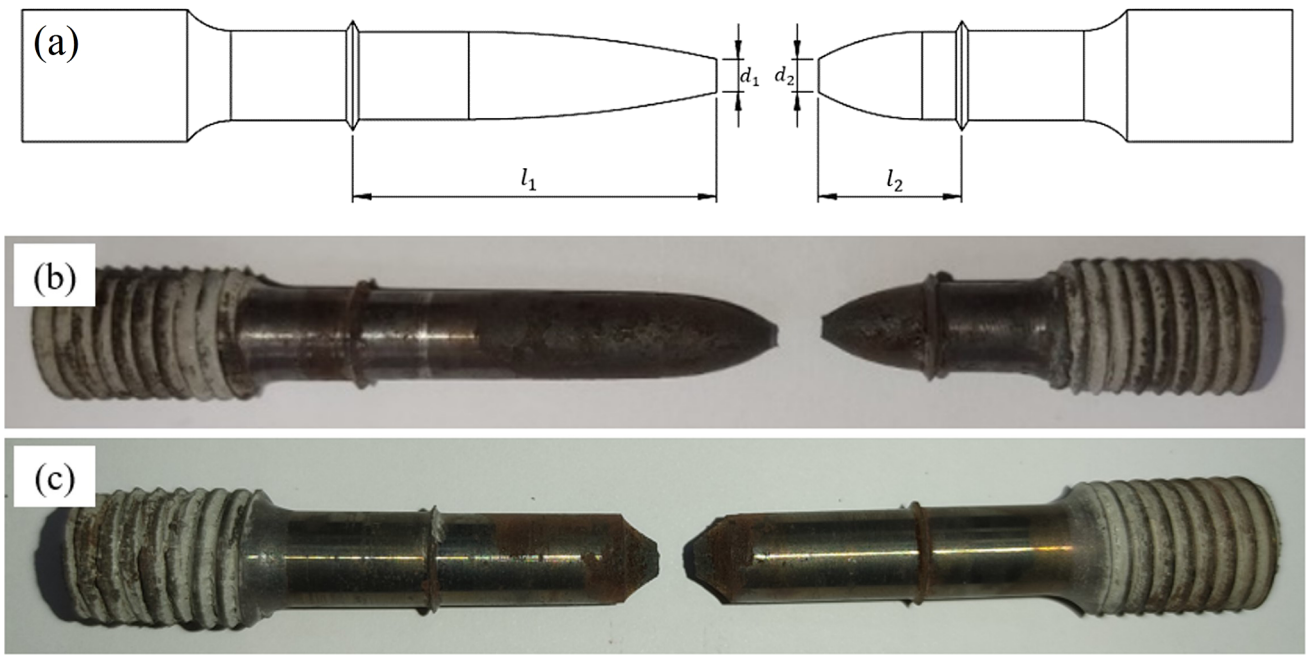

Fig. 6 (**a**) Schematic of a crept sample, (**b**) crept sample of a smooth specimen, (**c**) crept sample of a notched specimen

secondary phase. A steady creep strain rate was observed in the secondary stage. The development and destruction of the high dislocation density in the material occur at the same rate and contribute to this behaviour [22]. During the secondary stage, the creep damage develops continuously in the material, which reduces the creep strength and leads to the onset of the tertiary stage. In the tertiary stage, tensile instability or necking is observed, leading to a significant increase in strain rate up to fracture. The deformation of the specimen is recorded every 300 s during the creep test. Since fracture is an instantaneous process, the last data point in Fig. 7 does not represent the exact value of ductility. Although ductility is estimated by measuring the final deformation of the crept specimen, the unstable fracture process may contribute to the discrepancies in the measurement.

The creep rupture test was performed on a total of eight notched bar specimens of Grade 91 steel: four for blunt (acuity = 2.28) and four for medium (acuity = 4.56) notches. Similar to the smooth specimens, all notched bars

also show three different creep deformation stages (primary, secondary, and tertiary) (see Fig. 8), indicating the same deformation-controlled mechanism between two different specimens. Note that the creep curve for a notched bar is plotted based on axial displacement, not creep strain. This is due to the strain induced by the notch is not uniformly distributed along the gauge length, so the axial displacement may better represent the material deformation. In addition, the stress reported for the notched bar in Fig. 8 was calculated based on the area at the notch throat; thus, it is referred to as the net stress. At the same net stress level, the specimen with higher acuity tends to have lower values of primary, secondary, and tertiary deformation compared to the specimen with lower acuity. The same observation of lower displacement/deformation in all stages was also found when the net stress decreases from 240 to 210 MPa. Moreover, the tertiary deformation of medium notch is relatively small compared to the blunt notch. At a very long-term time, therefore, brittle-like fracture is anticipated. It should be noted that the presence of a notch is a geometric constraint that limits the deformation.

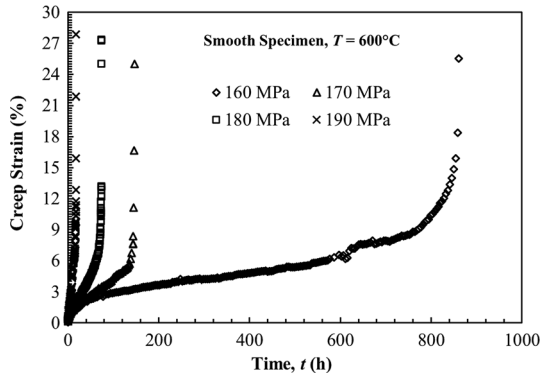

Fig. 7 Creep strain versus time for smooth specimen

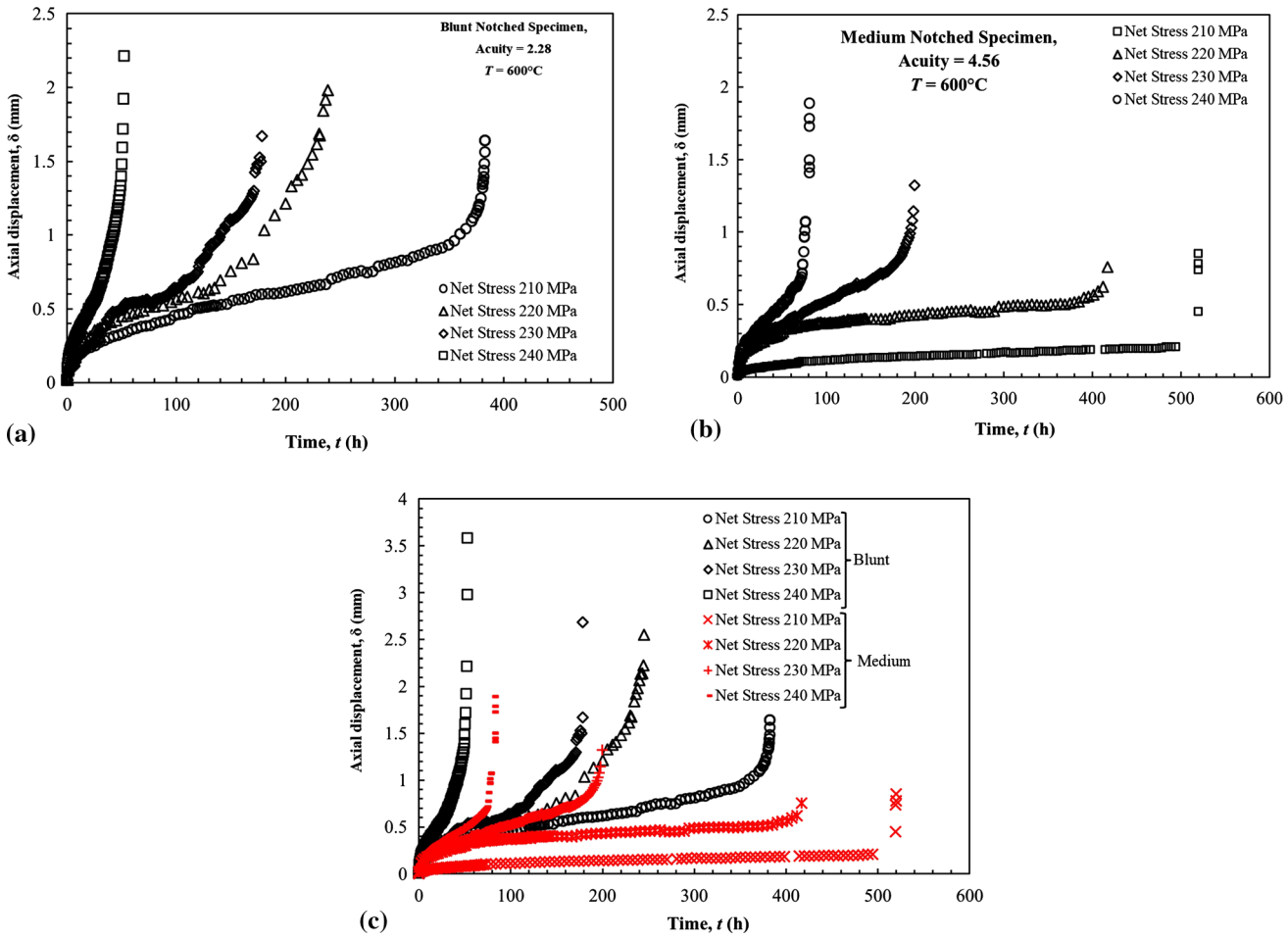

Fig. 8 Axial displacement against creep time (**a**) Medium notch, acuity = 4.56, (**b**) blunt notch, acuity = 2.28, (**c**) comparison between blunt and medium notch

Summary of the Creep Test

Tables 3 and 4 summarize the creep test results. Failure strain evaluated using Monkman–Grant (MG) ductility, elongation, and reduction of area (ROA) decrease as the applied stress decreases. At 190 MPa, failure strain (elongation), MG ductility, and ROA are 29%, 8.93%, and 94%, respectively. Meanwhile, at 160 MPa, the values are reduced to 21%, 4.6%, and 90%, respectively. There is an unexpected fluctuation of failure strain value for the stress of 170 MPa. This may be due to the unstable process of fracture. However, the data from other stress levels are sufficient to represent the overall trend of failure strain behavior.

Effect of Stress on Minimum Creep Strain Rate

Figure 9 shows the minimum creep strain rate as a function of net stress, σ. The solid line represents the best-fit power law curve obtained from the NIMS data. The minimum creep strain rate determined in the current study is also included in the figure. The minimum creep strain rate increases as the stress level increases. The boundary between the two regimes can be easily seen, and the intersection is marked at 125 MPa (0.5 S_y). According to the Norton law, the changes follow a power law relationship of the type $\dot{\varepsilon}_m = A\sigma^n$. At higher stresses, the value of n is 13.76, and at lower stresses, it is 5.84. The different value of n proves that the predominant creep mechanism is different in the two regimes. Based on the observed high-stress exponent, it can be assumed that dislocation creep acts as the primary creep deformation mechanism [23].

Relative Time Fraction of Each Creep Stage

Figure 10 illustrates the percentage of time spent on each stage of creep deformation at different stress levels of smooth specimens. Obviously, more than 80% of the material's life is spent in a steady-state or secondary stage, regardless of stress levels. The primary stage appears to be the shortest deformation, where the material spent only less than 10% of the total lifetime. The tertiary deformation is 13, 15, 16, and 14% at 160, 170, 180, and 190 MPa, respectively. Under these experimental conditions, the tertiary deformation appears to influence the overall rupture life, indicating that tensile instability is still present after uniform deformation in the secondary stage. However, it is believed that the deformation behaviour of Grade 91 steel behaves differently at extremely long periods than described in this work. This is due to localized damage that

Table 3 Summary of uniaxial creep experimental results of smooth specimen

Specimen type	Stress (MPa)	t_r (h)	ε_f (%)	ε_{MGf} (%)	ROA (%)
Smooth specimen	160	861	21.46	4.65	90.17
	170	148	36.08	6.10	90.35
	180	74	28.28	7.03	93.54
	190	18	29.64	8.93	94.75

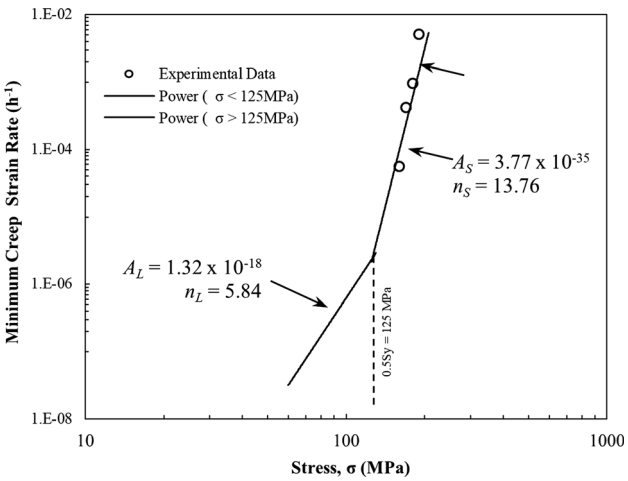

Fig. 9 Minimum creep strain rate versus stress

Table 4 Summary of uniaxial creep test results of notched specimen

Specimen type	Notch Radius (mm)	Notch acuity	Stress (MPa)	t_r(h)	ε_f (%)	ε_{MGf}(%)	ROA (%)
Blunt specimen	2.5	2.28	210	383	5.89	1.83	62.67
			220	245	5.73	1.62	69.91
			230	179	6.39	2.32	70.73
			240	53	6.64	2.41	71.57
Medium specimen	1.25	4.56	210	520	1.7	0.30	49.07
			220	417	3.11	0.60	32.35
			230	199	5.61	1.69	69.39
			240	81	9.75	1.44	72.13

has developed in the material, which has then resulted in localized constraint at the microstructural level. Increased material constraint resists material deformation. Therefore, it is expected that tertiary creep will not be observed during long-term creep.

Figure 11 shows the time frame of three different stages of creep deformation for notched bar specimens. Regardless of the ratio of notch acuity, the secondary stage controls the rupture life of the notched specimens. The trend of increasing time percentage was observed when the stress for both notches decreases from 240 to 210 MPa. Moreover, the primary creep deformation appears to be the shortest deformation among the three stages. Surprisingly, the tertiary stage of the blunt notch at 240 MPa lasts relatively long, occupying about 27% of the total lifetime. The percentage of time for tertiary deformation decreases to 16% when the stress is reduced to 210 MPa. This value is even higher than that found for smooth specimens. However, a direct comparison between smooth and notched bars is not possible at this point because of the inconsistency of applied stress. For a medium notch, the time for tertiary deformation tends to be shorter and negligible. The observation described in this section shows that secondary deformation is an important stage to consider, especially when developing a predictive model.

Effects of Net Stress on Failure Strain and Rupture Life

Figures 12 and 13 show the failure strain dependent (in terms of reduction of area and ductility) on net stress. From Fig. 12, only slight differences between the ROA values were observed for smooth specimens. The values vary

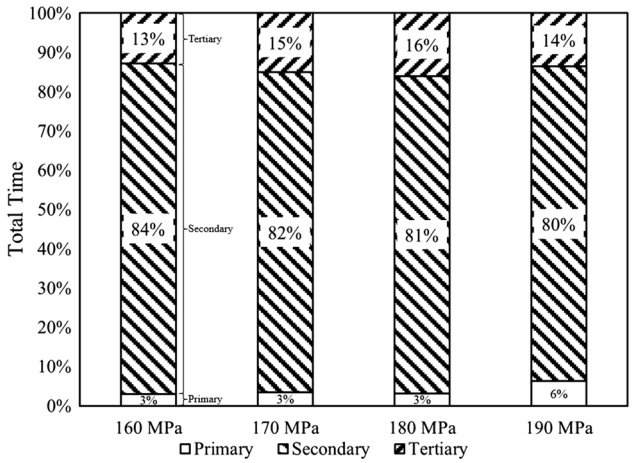

Fig. 10 Time fraction for each creep stage for smooth specimen

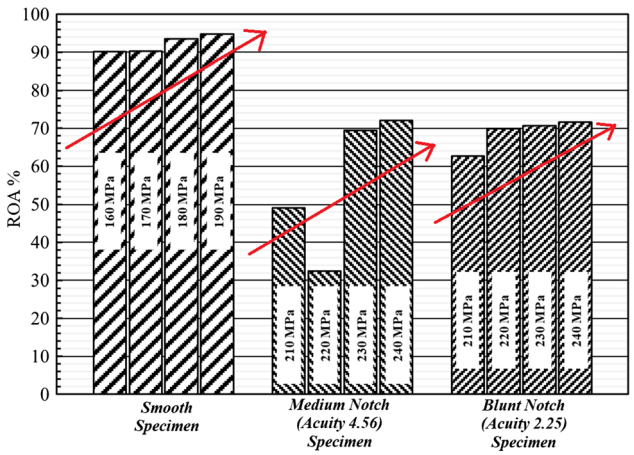

Fig. 12 Effect of net stress on ROA

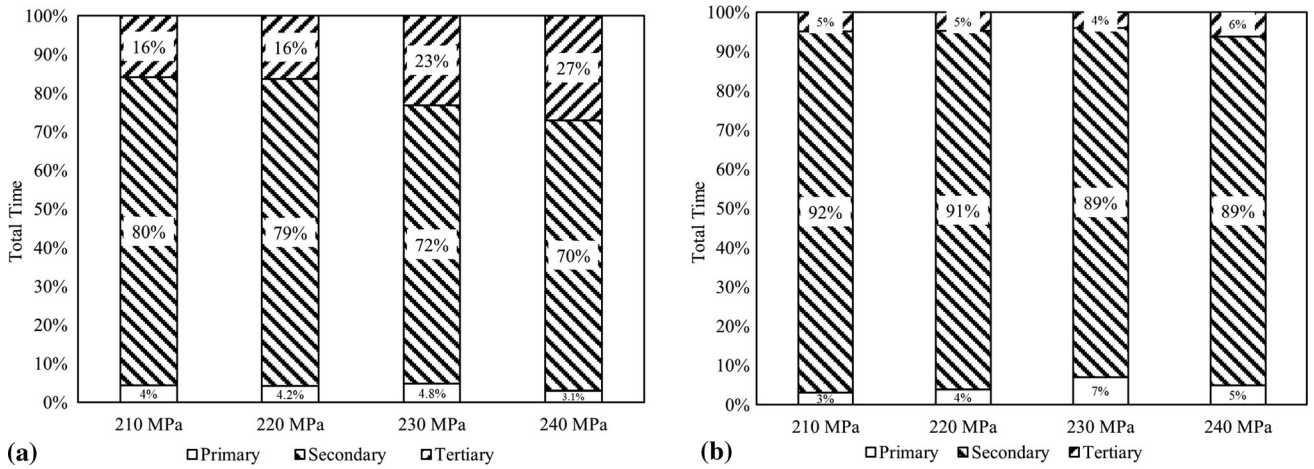

Fig. 11 Relative time fraction for each creep stage for notched specimen, (**a**) blunt notch; (**b**) medium notch

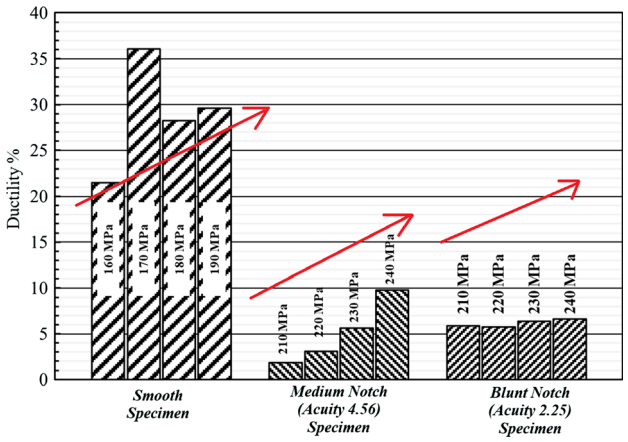

Fig. 13 Effect of net stress on ductility

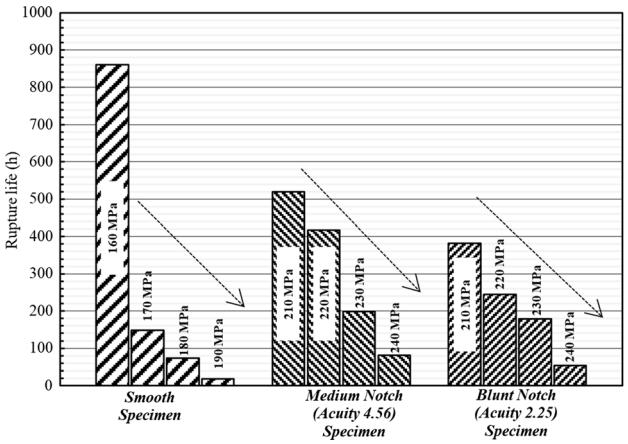

Fig. 14 Effect of net stress on rupture life for all tested specimens

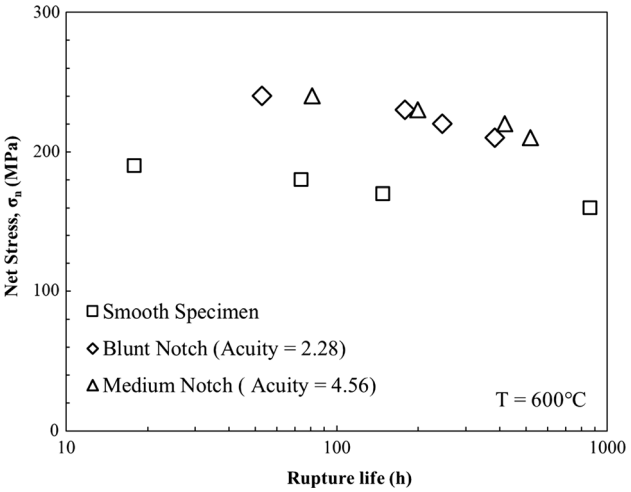

Fig. 15 Influence of net section stress on time to rupture showing the notch strengthening phenomenon

between 90 and 94% at stress levels between 160 and 190 MPa. A similar trend was observed for the acuity level of 2.28, while a significant change in the ROA value was observed for the acuity level of 4.56. It is also evident from the figures that the ROA value increases with increasing stress for all specimens (indicated by arrows). An unexpected result was obtained for the 220 MPa stress level in the case of acuity 4.56, where the ROA drops to 32%, while at 210 MPa, it is 49%. A possible explanation for this could be the unstable process of fracture. Figure 13 shows the effects of net stress on ductility (elongation). In general, ductility increases with increasing stress, while smooth specimens have higher ductility than notched specimens. For smooth specimens, ductility increased from 21 to 29% at stresses between 160 and 190 MPa. Surprisingly, ductility at 170 MPa was found not to follow this trend. For blunt-notched specimens, ductility increased from 5.8 to 6.6%, and for medium-notched specimens, from 1.8 to 9.7% at stress levels from 210 to 240 MPa.

Figure 14 plots the rupture data for smooth and notched specimens against net stress. It can be seen that the medium notch (acuity = 4.56) has a higher creep life than the blunt notch (acuity = 2.28) at the same stress level. At the acuity level of 4.56, the rupture life is 520, 417, 199, and 81 h at stresses of 210, 220, 230, and 240 MPa, respectively, while at an acuity level of 2.28, the rupture life is 383, 245, 179, and 53 h at the same stress range. The time to rupture for the smooth and notched specimens with two notch acuities is shown in Fig. 15. The rupture life of all notched specimens shows a longer time to rupture than smooth specimens when subjected to the same net-section stress level. This phenomenon indicates that the notched specimens of Grade 91 steel exhibit a significant notch strengthening effect. At higher stress levels, the notched specimen exhibited longer rupture duration of the smooth specimen. This behaviour is consistent with the findings of Goyal [10]. It reflects the fact of "notch strengthening" that occurs because the equivalent the von-Mises stress is reduced by the notch. This property is more pronounced in ductile materials [7].

Effects of Representative Stress on Rupture Life

The life of notched bar depends on the various stress components. Therefore, the use of net stress is not an accurate approach for comparing the time of creep failure between a uniaxial specimen and the notched bar. For this reason, a concept known as "representative stress" was introduced. This concept has been used to predict the creep failure time of notched bars and is based on the knowledge that failure is governed by a combination of MPS and von-Mises stress [24]. In this study, skeletal stress is used to estimate the von-Mises and MPS stress of the notched bar. Skeletal stress is, by definition, the component of stress at

the skeletal radius where the level of stress does not change while the creep stress exponent varies. According to Webster [24], the values for the ratio between skeletal stress and net stress for blunt and medium notches are given in Table 5.

Figure 16 shows the plot of skeletal von-Mises and MPS against rupture life for notched specimens. The best-fit curves (solid line) for smooth specimens are also included in both plots for comparison. From Fig. 16b, the plot of maximum principal skeletal stress does not agree with the uniaxial test results. In contrast, the uniaxial and notched bar rupture data are well correlated when the skeletal von-Mises stress is employed (see Fig. 16a). This proves that the von-Mises stress controls the rupture life.

Table 5 Representative stresses of notched specimen

Specimen type	Notch radius (mm)	Notch acuity *(d/R)*	$\frac{\sigma^*_{VM}}{\sigma_{net}}$	$\frac{\sigma^*_m}{\sigma_{net}}$	$\frac{\sigma^*_1}{\sigma_{net}}$
Blunt notch specimen	2.50	2.25	0.80	0.50	1.04
Medium notch specimen	1.25	4.56	0.73	0.60	1.08

Influence of Triaxiality on Creep Failure

It is well known that creep ductility is highly associated with multiaxial stresses. Numerous void growth models, including Rice and Tracey [17], Cocks and Ashby [18], and Spindler [19], can be used to predict this relationship. These models imply the relationship of multiaxial to uniaxial ductility as a function of hydrostatic and equivalent stresses, referred to as triaxiality. As shown in Fig. 17, the multiaxial creep ductility models were compared with the test results for both notched specimens. The triaxiality of the stress in the test data was determined using the skeletal point analysis tabulated in Table 5. The present experimental creep data are insufficient to determine the power-law/stress exponent. Therefore, the creep exponent was

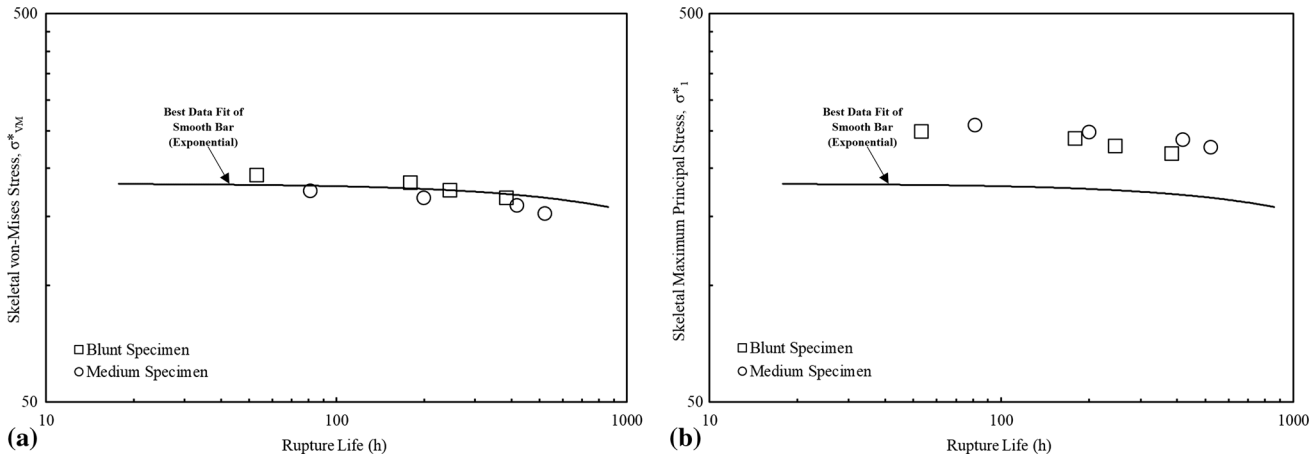

Fig. 16 (**a**) Skeletal von-Mises stress versus rupture life, (**b**) skeletal maximum principal stress versus rupture life

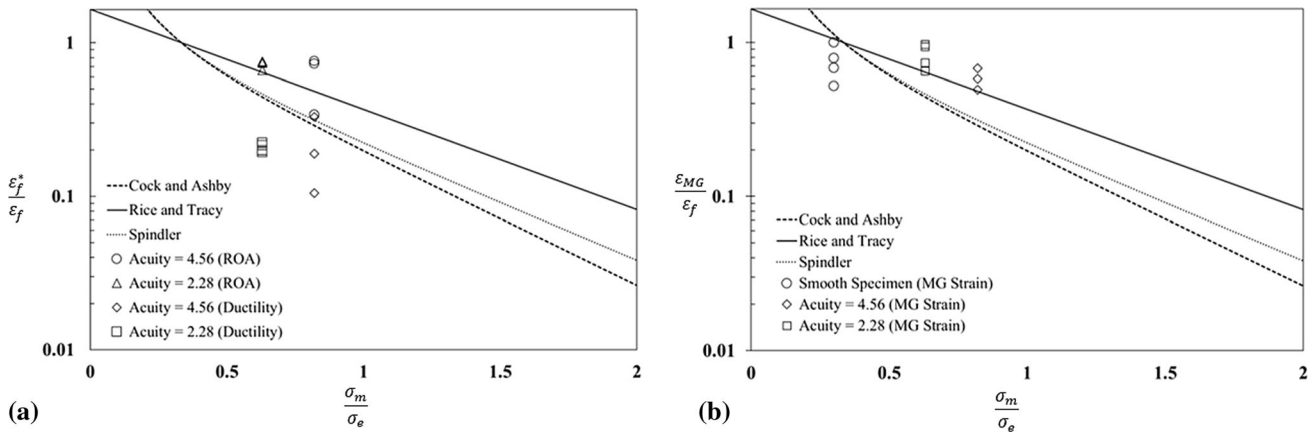

Fig. 17 Influence of triaxiality on creep failure strain at 873 K (**a**) Multiaxial stress, (**b**) Monkman grant

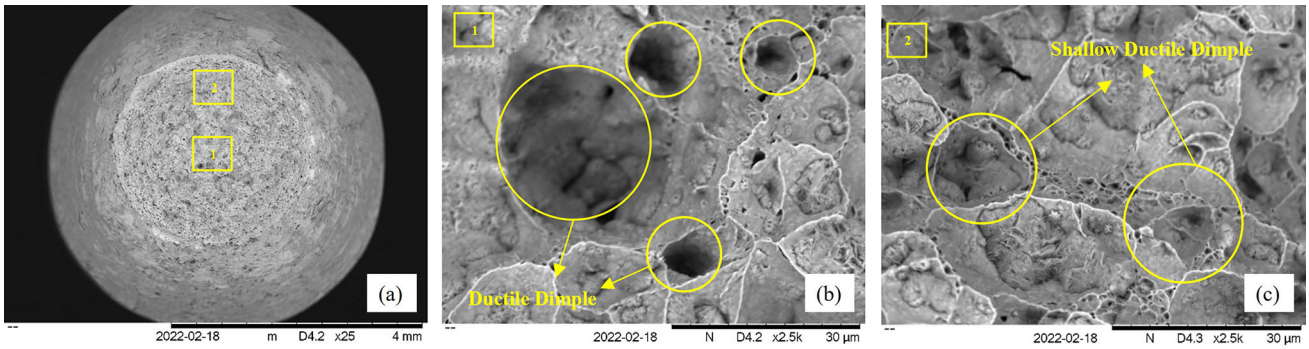

Fig. 18 Scanning electron microscopic presentation of notch specimen (Blunt) on (**a**) rupture surface, (**b**) middle of the notch throat, (**c**) near the notch root at the stress level of 230 MPa at 873 K

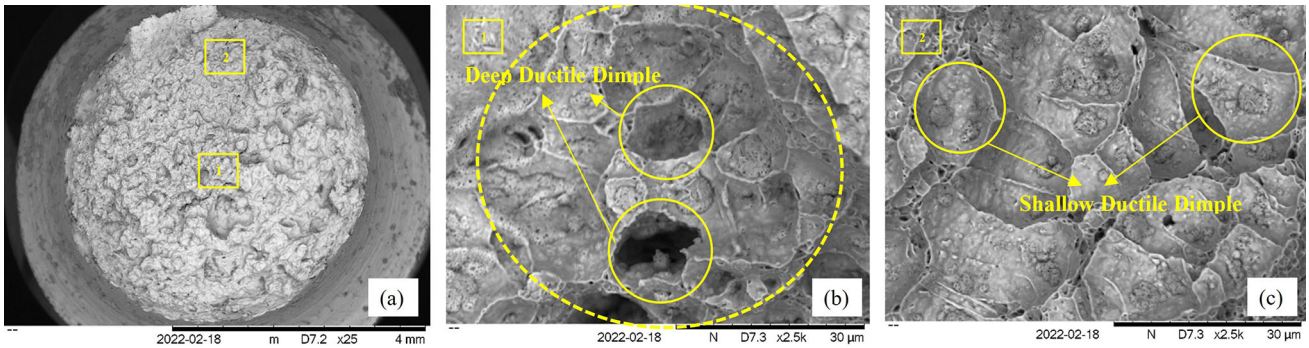

Fig. 19 Scanning electron microscopic presentation of notch specimen (medium) on (**a**) rupture surface, (**b**) middle of the notch throat, (**c**) near the notch root at the stress level of 220 MPa at 873 K

determined using data from NIMS [25]. A creep exponent of 13 was used for the analysis.

As seen in Fig. 17, Rice and Tracey's model fits the data quite well at a lower triaxiality except for acuity 2.28 in terms of ROA, but Cocks and Ashby, and Splinder's models overestimate it. It is worth noting that Rice and Tracey's model does not rely on the creep exponent because it is based on fully plastic material properties. As can be seen in Fig. 16, most of the test data is above the ROA-based failure strain prediction models. Thus, the model may have overestimated the test result. Attempting to extract the multiaxiality term from the curves will lead to further errors and make the whole technique indefinable since the data is scattered. Another attempt was made to analyze the multiaxiality using the Monkman–Grant failure strain. Monkman and Grant were the first to identify a correlation between time to rupture and minimum creep strain rate [26]. It can be described as the total uniaxial strain at the secondary stage. For both notched specimens, all void growth models underestimate the prediction except for Rice and Tracey.

Fractographic Examination

Figures 18 and 19 show the SEM micrograph of the fracture surface of the blunt- and medium-notched specimens at the stress level of 230 MPa and 220 MPa, respectively. For the blunt-notched specimen, the area near the center of the notch shows deep ductile dimples. Meanwhile, the area near the root shows a nearly flat surface having shallow dimples. In addition, a similar fracture of the ductile dimple was also observed in the medium-notched specimens (see Fig. 19). A relatively flat surface with shallow dimples can be seen near the root compared to the center. The ductility of the material can be compared in terms of the shape and depth of the dimple. Deep conical dimples are known to form naturally during high ductile fracture, which indicates that when crack resistance increases, the relative apparent size and depth of dimples at the fracture surface also increase [27]. These findings suggest that for the notched specimen, the center experiences more plastic deformation than the area near the notch root. These results further support the idea that the stress distribution along the notch ligament varies due to the notch constraint. Moreover, triaxiality plays an important role in creep ductility [28].

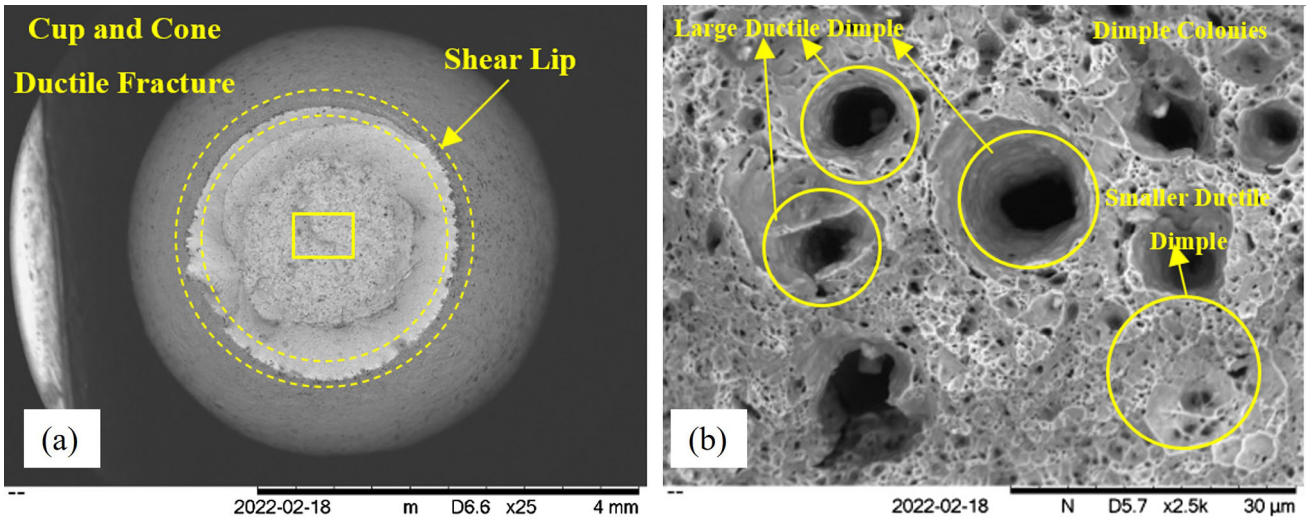

Fig. 20 Scanning electron microscopic presentation of the smooth specimen on (**a**) rupture surface, (**b**) middle of the throat at the stress level of 180 MPa at 873 K

Higher triaxiality (causes lower ductility) occurs between the center and the notch root. It is evident from these findings that the ductility was reduced due to the notch constraint. This could be due to the limited plastic deformation of voids. Consequently, less plasticity is observed near the notch root in the case on medium notch.

Figure 20 shows the SEM micrograph of the fracture surface of a smooth specimen tested at 180 MPa. A typical cup-cone fracture and shear lip can be clearly seen. Further examination revealed that the dimple colonies consisting of inhomogeneous (different sizes) ductile dimples are speared all over the fracture area. Moreover, the presence of ductile dimples indicates the formation and collection of micro-voids. Deep dimples can be attributed to higher ductility and longer creep life [29].

Conclusion

The creep behavior of the Grade 91 steel under the uniaxial and multiaxial stress state has been determined in this paper. Two types of notched specimens with different acuities were used, and the results were compared against the uniaxial creep data. It was found that the notched specimens exhibited a longer creep life than the smooth specimens, which indicates the "notch strengthening" effect. Also, all the specimen shows decreasing creep rupture life with the increase of stress and increasing failure strain (ductility and reduction of area) when the stress level increases. In addition, it was found out that the von-Mises stress governs the rupture life of the material under the tested stress level. The compatibility analysis of creep behavior with the void-growth model shows fewer accuracies. Fractographic analysis showed that compared to the region at the centre, the region near the notch root has shallow dimples, indicating less plastic deformation for the notched specimen. For the smooth specimens, the investigation revealed that the ductile dimples were predominant during fracture.

Acknowledgments The authors would like to express gratitude to the Ministry of Higher Education (MOHE) Malaysia and University Malaysia Pahang for funding this research under the Fundamental Research Grant Scheme FRGS/1/2019/TK03/UMP/02/2 (RDU1901107) and Internal Grant RDU220361, respectively.

References

1. W.G. Kim, H.Y. Lee, H.U. Hong, Evaluation of tension and creep rupture behaviors of long-term exposed P91 steel in a supercritical plant. Eng. Fail. Anal. **116**, 104736 (2020). https://doi.org/10.1016/j.engfailanal.2020.104736
2. F. Abe, "Development of creep-resistant steels and alloys for use in power plants," in *Structural Alloys for Power Plants*, Elsevier, 2014, pp. 250–293. doi: https://doi.org/10.1533/9780857097552.2.250.
3. F. Ren, X. Tang, Mechanical properties of Grade 91 steel at high temperatures. J. Phys. Conf. Ser. **1168**(2), 022013 (2019). https://doi.org/10.1088/1742-6596/1168/2/022013
4. L. Zhao, N. Alang, K. Nikbin, Investigating creep rupture and damage behaviour in notched P92 steel specimen using a microscale modelling approach. Fatigue Fract. Eng. Mater. Struct. **41**(2), 456–472 (2018). https://doi.org/10.1111/ffe.12713
5. D. Barbera, H. Chen, Y. Liu, Advances on creep–fatigue damage assessment in notched components. Fatigue Fract. Eng. Mater. Struct. **40**(11), 1854–1867 (2017). https://doi.org/10.1111/ffe.12603

6. X. Xu, G.Z. Wang, F.Z. Xuan, S.T. Tu, Effects of creep ductility and notch constraint on creep fracture behavior in notched bar specimens. Mater. High Temp. **33**(2), 198–207 (2016). https://doi.org/10.1080/09603409.2016.1144498
7. K.C. Sahoo, V.D. Vijayanand, S. Goyal, P. Parameswaran, K. Laha, Influence of temperature on multiaxial creep behaviour of 304HCu austenitic stainless steel. Mater. Sci. Technol. (United Kingdom). **35**(18), 2181–2199 (2019). https://doi.org/10.1080/02670836.2019.1664707
8. S. Goyal, K. Laha, C.R. Das, M.D. Mathew, Analysis of creep rupture behavior of Cr-Mo ferritic steels in the presence of notch. Metall. Mater. Trans. **46**(1), 205–217 (2015). https://doi.org/10.1007/s11661-014-2609-2
9. J. D. Parker and J. A. Siefert, "Creep fracture in tempered martensitic steels," vol. 3, no. 1, pp. 1–7, 2018, doi: https://doi.org/10.15406/ipcse.2018.03.00068.
10. S. Goyal, K. Laha, C. R. Das, S. Panneerselvi, and M. D. Mathew, "Effect of constraint on creep behavior of 9Cr-1Mo steel," *Metall. Mater. Trans. A Phys. Metall. Mater. Sci.*, vol. 45, no. 2, pp. 619–632, 2014, doi: https://doi.org/10.1007/s11661-013-2025-z.
11. D.S. Liu, D.X. Zhang, J.W. Liang, Z.X. Wen, Z.F. Yue, Prediction of creep rupture life of a V-notched bar in DD6 Ni-based single crystal superalloy. Mater. Sci. Eng. A. **615**, 14–21 (2014). https://doi.org/10.1016/j.msea.2014.07.006
12. W.G. Kim, J.Y. Park, S.J. Kim, E.S. Kim, J. Jang, Improvement of long-term creep life extrapolation using a new master curve for Grade 91 steel. J. Mech. Sci. Technol. **32**(9), 4165–4172 (2018). https://doi.org/10.1007/s12206-018-0814-4
13. D.P.R. Palaparti, E.S. Isaac, B.K. Choudhary, M.D. Mathew, Creep Properties of Grade 91 Steel Steam Generator Tube at 923K Creep Properties of G Grade 91 Steel Steam Generator Tu ube at 923K. Procedia Eng. **55**(December), 70–77 (2013). https://doi.org/10.1016/j.proeng.2013.03.221
14. T. Tian, Z. Hao, C. Ge, X. Li, S. Peng, and C. Jia, "Effects of stress and temperature on creep behavior of a new third-generation powder metallurgy superalloy FGH100L," *Mater. Sci. Eng. A*, vol. 776, no. January, p. 139007, 2020, doi: https://doi.org/10.1016/j.msea.2020.139007.
15. I.J. Perrin, D.R. Hayhurst, Continuum damage mechanics analyses of type IV creep failure in ferritic steel crossweld specimens. Int. J. Press. Vessel. Pip. **76**(9), 599–617 (1999). https://doi.org/10.1016/S0308-0161(99)00051-4
16. Y. Chang, H. Xu, Y. Ni, X. Lan, H. Li, Research on representative stress and fracture ductility of P92 steel under multiaxial creep. Eng. Fail. Anal. **59**, 140–150 (2016). https://doi.org/10.1016/j.engfailanal.2015.09.011
17. J.R. Rice, D.M. Tracey, On the ductile enlargement of voids in triaxial stress fields*. J. Mech. Phys. Solids. **17**(3), 201–217 (1969). https://doi.org/10.1016/0022-5096(69)90033-7
18. A.C.F. Cocks, M.F. Ashby, On creep fracture by void growth. Prog. Mater. Sci. **27**(3–4), 189–244 (1982). https://doi.org/10.1016/0079-6425(82)90001-9
19. M.W. Spindler, The multiaxial creep ductility of austenitic stainless steels. Fatigue Fract. Eng. Mater. Struct. **27**(4), 273–281 (2004). https://doi.org/10.1111/j.1460-2695.2004.00732.x
20. ASTM E139–11, "Standard Test Methods for Conducting Creep , Creep-Rupture , and Stress-Rupture," *Order A J. Theory Ordered Sets Its Appl.*, no. August 2000, pp. 1–12, 2003, doi: https://doi.org/10.1520/E0139-11.
21. ASTM E292–18, "Standard Test Methods for Conducting Time-for-Rupture Notch Tension Tests of Materials," *Order A J. Theory Ordered Sets Its Appl.*, vol. 83, no. Reapproved, pp. 1–12, 2009, doi: https://doi.org/10.1520/E0292-09E01.2.
22. T. Sakthivel et al., Creep rupture behavior of 9Cr–1.8W–0.5Mo–VNb (ASME grade 92) ferritic steel weld joint. Mater. Sci. Eng. A. **591**, 111–120 (2014). https://doi.org/10.1016/j.msea.2013.10.071
23. L. An, Q. Xu, D. Xu, and Z. Lu, "Review of creep deformation and rupture mechanism of P91 alloy for the development of creep damage constitutive equations under low stress level," *Proc. WORLDCOMP2013—The 2013 Int. Conf. Sci. Comput. CSREA Press.*, pp. 184–187, 2013.
24. G.A. Webster et al., A code of practice for conducting notched bar creep tests and for interpreting the data. Fatigue Fract. Eng. Mater. Struct. **27**(4), 319–342 (2004). https://doi.org/10.1111/j.1460-2695.2004.00765.x
25. K. Sawada et al., Catalog of NIMS creep data sheets. Sci. Technol. Adv. Mater. **20**(1), 1131–1149 (2019). https://doi.org/10.1080/14686996.2019.1697616
26. V. Sklenicka, K. Kucharová, P. Král, M. Kvapilová, J. Dvorák, Applicability of empirical formulas and fractography for assessment of creep life and creep fracture modes of tempered martensitic 9%Cr steel. Kov. Mater. **55**(2), 69–80 (2017). https://doi.org/10.4149/KM_2017_2_69
27. I. Konovalenko, P. Maruschak, O. Prentkovskis, Automated method for fractographic analysis of shape and size of dimples on fracture surface of high-strength titanium alloys. Met. **8**(3), 161 (2018). https://doi.org/10.3390/MET8030161
28. I.U. Ferdous, N.A. Alang, J. Alias, S.M. Nadzir, Numerical prediction of creep rupture life of ex-service and as-received grade 91 steel at 873 K. Int. J. Automot. Mech. Eng. **18**(3), 8845–8858 (2021). https://doi.org/10.15282/ijame.18.3.2021.01.0678
29. K. Guguloth, N. Roy, Study on the creep deformation behavior and characterization of 9Cr-1Mo-V-Nb steel at elevated temperatures. Mater. Charact. **146**(May), 279–298 (2018). https://doi.org/10.1016/j.matchar.2018.10.011